Journal of Materials Chemistry A

ROYAL SOCIETY OF CHEMISTRY

PAPER

View Article Online
View Journal | View Issue

Cite this: J. Mater. Chem. A, 2024, 12, 8972

Energy-efficient UV-to-NIR active smart electrochromic tetrabenzofluorene molecules†

Panichiyil V. Navya and Srinivasan Sampath *

Electrochromic (EC) smart windows are considered a profitable energy conservation technology in residential and commercial buildings. These windows can dynamically adjust their opacity or tint in response to external factors such as temperature, sunlight, or user input. External bias produces charged species capable of absorbing light in the electromagnetic spectrum, eventually regulating heating, cooling, and lighting inside buildings. Another fundamental property of EC devices is their ability to store charge from input currents. Here, three new classes of tetrabenzofluorene derivatives are reported, which show excellent EC properties in terms of EC contrast (40–50%), coloration efficiency (above 100 $cm^2\ C^{-1}$), and response time (5 s). Furthermore, EC devices function in three states: solid, solution, and gel states, and can also store the applied charge proficiently. The devices showed excellent cycling stability (300 cycles), capacity retention (95–100%), and moderately slow discharging; *i.e.*, the solid-state device produced an open circuit potential close to 1.2 V and discharged to 0.6 V in 2000 s. Moreover, the charging and discharging process can be monitored visually by the change in color of the EC material. The design strategy, synthesis, detailed optical, electrochromic, and spectroelectrochemical characterization, proof-of-concept smart window fabrication, and energy storage studies are presented.

Received 3rd November 2023
Accepted 1st March 2024

DOI: 10.1039/d3ta06726b

rsc.li/materials-a

1. Introduction

The increasing demand for cooling commercial and residential buildings and modern lifestyle choices has contributed to high energy consumption. Reducing energy usage in cooling buildings is crucial for lowering energy bills and mitigating the environmental impacts associated with increased energy use, including greenhouse gas emissions and resource depletion. Global warming and climatic changes are the major concerns the current era faces. The growing demand for developing cost-effective and high-performance energy storage technologies has gained scientific attention and produced remarkable progress in electrochemical energy storage technologies.[1] Various organic–inorganic hybrid materials, small molecules, metal oxides, and conjugated polymers have emerged, which function as electrode materials for batteries or supercapacitors.[2] Hence, developing energy-efficient technologies that regulate heating and cooling at low energy expenditure is critical.

In this direction, electrochromic (EC) molecules that can switch their optical properties, such as absorbance or transmittance, in response to external potential are highly explored because they absorb light in the UV-visible and NIR regions of the electromagnetic spectrum, thereby controlling the lighting as well as solar heat gain inside buildings.[3] As technology advances, researchers successfully integrate energy storage functionality and electrochromic properties in a single unit. The EC device (ECD) can store charge from input currents and reutilize this stored energy to power electronic appliances. Combining energy storage and electrochromic technology aligns with sustainability goals by lessening reliance on fossil fuels, enhancing energy efficiency, and boosting renewable energy integration.[4] Several research groups have developed these EC energy storage devices using metal oxide-based or viologen derivatives.[5,6]

However, inorganic materials provide better performance in terms of capacitance and performance; their band gap tuning is challenging, making it difficult to tune the optical properties of electrochromes. Thus, organic EC materials are widely explored.[7] Various design strategies have been developed to create new EC materials to improve the contrast ratio, coloration efficiency, and stability of the devices for real-time applications. This can be achieved by controlling the extent of conjugation, tuning the molecular backbone planarity by creating or relieving the steric hindrance, incorporating donor–acceptor units in the building blocks, copolymerization with electroactive heteroatom units, and forging composites by integrating with chromophore units.[8–12] Though quick responsive, developing high contrast, wide color change, and highly reversible ECDs with energy storage properties is still challenging.

In this work, we developed three new classes of multifunctional smart molecules capable of absorbing UV-visible and NIR

Department of Materials Science, School of Technology, Central University of Tamil Nadu, Thiruvarur, 610005, India. E-mail: srinivasansampath@cutn.ac.in; sampathsrinivasan@yahoo.com

† Electronic supplementary information (ESI) available. See DOI: https://doi.org/10.1039/d3ta06726b

rays, showing electrochromism and energy storage properties. Electrochromes function in three states: solid, solution, and gel. The energy storage characteristics of the newly synthesized molecules are thoroughly studied and found to be highly efficient in terms of capacity retention (95–100%), coloration efficiency, and EC contrast. To the best of our knowledge, no research groups have reported the energy storage and EC properties of tetrabenzofluorene (TBF) derivatives; viologen and amine derivatives are small molecules showing such multifunctionality. Moreover, no report has been published investigating the effect of positional isomers in electrochromism. Here, we report the synthesis, electrochemical, optical, and energy storage properties of TBF-based regioisomers and acceptor–donor–acceptor (ADA) EC molecules.

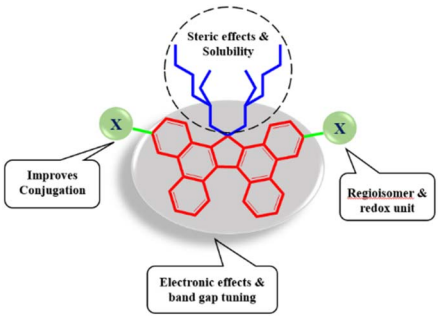

Fig. 1 The design strategy of electrochromic tetrabenzofluorene derivatives *via* band gap tuning by increasing conjugation, anchoring with thiophene derivatives, and improving the solubility by incorporating branched alkyl groups.

2. Results and discussion

2.1 Design principles

The synthesis of three novel solution-processable extended π-conjugated anodically coloring electrochromic organic small molecules is reported, which switch their color from a transparent to a vibrant colored state. The optical absorption of the molecules in the neutral state can be controlled by fine-tuning the conjugation length of the molecular backbone, which depends upon the energy levels of the highest occupied molecular orbital (HOMO) as well as the lowest unoccupied molecular orbital (LUMO). The TBF molecule was taken as the core unit because the conjugation in the core molecule plays an essential role in modifying the optical band gap. Compared to conjugated polymers, using small molecules as the core can precisely bring the neutral state absorption in the UV region.

The extent of the conjugation can be enhanced by integrating suitable heterocycles with the core. Thiophene derivatives are found to be an efficient class of EC moieties due to their redox nature; thus, thiophene units were incorporated into the molecular backbone. The equilibrium geometry, steric hindrance, dihedral angle between the core and the substituent, and the functional unit's electronic effects are crucial in defining the optical band gap. So, two positional/regioisomers, 2-thienyl and 3-thienyl derivatives, were attached to the TBF unit to examine the absorption profile in the neutral state. Compared to the 2-thienyl, the 3-thienyl group may deliver a blue shift in the absorption due to the decrease in effective conjugation length resulting from the orientation of the thiophene ring by disrupting the planarity of the molecules. Apart from these positional isomers, an ADA system was also created to investigate the impact of such systems on coloration efficiency and EC contrast. This was accomplished by integrating electron-withdrawing acetyl groups in the fifth position of the 2-thienyl derivative of TBF. Thus, the 2- and 3-thienyl derivatives of TBF act as the donor systems; however, the introduction of the acetyl moiety produces an electron-withdrawing effect on the electron-rich bisthiophene-TBF unit and results in an A–D–A system. Another significant factor that one should consider while designing the electrochrome is solubility. Solubility plays an important role in device fabrication.[10,12–16] 2-Ethylhexyl groups were chosen because they will provide solubility and are large enough to produce a steric effect on the electrochrome, and the design strategy towards the synthesis of TBF-based electrochromes is shown in Fig. 1.

The above-mentioned geometrical arrangement of the regioisomers was verified by optimizing the geometries using density functional theory (DFT) calculations, and the optimized geometries are illustrated in Fig. S30.† In TBFT1, the dihedral angle between the tetrabenzofluorene core and the 3-thienyl substituent is 21.13° and 20.47°, which is higher than the dihedral angle between the core and 2-thienyl substituent (6.83° and 0.04°) in TBFT2. This higher dihedral angle in TBFT1 substantiates the out-of-plane orientation of the 3-thienyl substituent in a different plane. Meanwhile, in TBFT2 and TBFT3, the core and the substituents are in the same plane, leading to an enhanced conjugation. Thus, compared to TBFT1, the 2-thienyl substituted derivative, TBFT2, will have an extended conjugation since it has a relaxed geometry. Furthermore, the alkyl groups also strain the geometry due to their bulkiness, as we can see that the bond angles between C2 and C1 are in the range of 127° in all these structures. Thus, the geometry optimization results are in agreement with the expected orientation of the molecules.

2.2 Synthesis of electrochromes

Electrochromes TBFT1–3 were synthesized according to the procedure shown in Scheme 1. The two regioisomers of TBF (TBFT1 and TBFT2) and ADA systems (TBFT3) are synthesized by hooking an electron-withdrawing 5-acetyl-2-thienyl group. The TBF core (1) was synthesized following the previously reported procedure (Scheme S1†).[17,18] Since compound 1 has poor solubility, it is subjected to alkylation with a branched alkyl chain, 2-ethylhexyl group, and compound 2 was obtained. It was then subjected to bromination using *N*-bromosuccinimide (NBS) in *N*,*N*-dimethylformamide (DMF) solvent, and TBF-Br was obtained with an 80% yield. Finally, the redox-active heterocycles were incorporated into TBF-Br through a series of Suzuki-coupling reactions using the corresponding boronic acids and tetrakis(triphenylphosphine)palladium(0) as the catalyst. The synthetic details are provided in the experimental section in the ESI.† These molecules were purified and

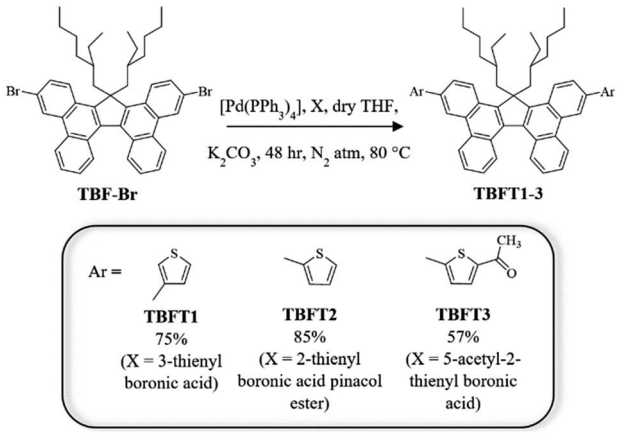

Scheme 1 Synthetic route for the preparation of the electrochromes TBFT1–3.

characterized by ^{1}H and ^{13}C (1D and 2D) NMR spectroscopy, ATR-FTIR, and mass spectrometry (Fig. S1–27 and S29†). The thermal stability of the compounds is studied using thermogravimetric analysis (TGA). The regioisomers, TBFT1 and TBFT2, are stable up to 400 °C, as seen in Fig. S28.† However, the ADA system TBFT3 is thermally stable up to 350 °C, and the instability above 350 °C may be due to the decomposition of acetyl groups.

2.3 Photophysical studies

The UV-visible absorption spectra of the electrochromes in chloroform are depicted in Fig. 2a. Due to the dihedral angle resulting from the out-of-plane frontage of the 3-thienyl group, the conjugation length across the molecular backbone (TBFT1) reduced and shifted the absorption in the UV region, centred at 390 nm as intended. At the same time, TBFT2 and TBFT3 absorb in the visible region with an absorption maximum (λ_{max}) of 403 nm and 433 nm, respectively. As expected, the acceptor moieties in TBFT3 improved the conjugation and produced a red shift in the absorption. The absorbance values at λ_{max} of TBFT1 (molar extinction coefficient, $\varepsilon = 68\,000\ m^{-1}\ cm^{-1}$) and TBFT2 ($\varepsilon = 65\,200\ m^{-1}\ cm^{-1}$) are nearly the same, whereas the acceptor units enhanced the absorbance of TBFT3 ($\varepsilon = 86\,900\ m^{-1}\ cm^{-1}$). Consequently, the color of the neutral species varied from transparent/colorless (TBFT1), pale yellow (TBFT2), and bright yellow (TBFT3).

The fluorescence spectra of the compounds are recorded and depicted in Fig. 2b. The emission intensities of TBFT1 and TBFT2 are similar, whereas TBFT3 showed less fluorescence; these observations can be illustrated due to the higher rate of non-radiative emission compared to radiative emission in TBFT3. In TBFT3, the presence of electron-withdrawing groups in the TBF core may decrease the quantum yield by increasing the non-radiative pathway. However, TBFT1 and TBFT2 gave outstanding quantum yield values. Both the molecules have quantum yields of above 0.80 and lifetime values of more than 1.5 ns, compared to TBFT3. The photophysical parameters such as absorption and emission maxima, quantum yield (Φ_f), lifetime (τ), radiative rate constants (k_r), and non-radiative rate constants (k_{nr}) are summarized in Table 1.[19] The photophysical studies suggest that the molecules TBFT1 and TBFT2 can be useful in fabricating light-emitting devices.

2.4 Spectroelectrochemical studies

Electrochemical studies were performed in a 3-electrode setup using 0.1 M tetrabutylammonium hexafluorophosphate ($TBAPF_6$) as the supporting electrolyte, a glassy carbon working electrode, a calomel electrode as the reference electrode, and Pt wire as the counter electrode in dichloromethane (DCM) solvent. The cyclic voltammograms (CV) of the compounds are given in Fig. 2c, and all three compounds showed two reversible redox couples in the potential range of 0–2 V. The onset oxidation potentials of the first oxidation peak of TBFT1–3 are 1.26, 1.25, and 1.36 V, respectively. Furthermore, the electrochemical stability of the compounds is examined by recording CV for continuous 300 cycles, and the results confirm the excellent stability of the molecules (Fig. S32†). The differential pulse voltammograms (DPV) of the compounds are given in Fig. S31,† and the CV of the compounds at different scan rates is shown in Fig. S33.† The redox potentials and the corresponding HOMO and LUMO values are calculated and briefed in Table 1.[20]

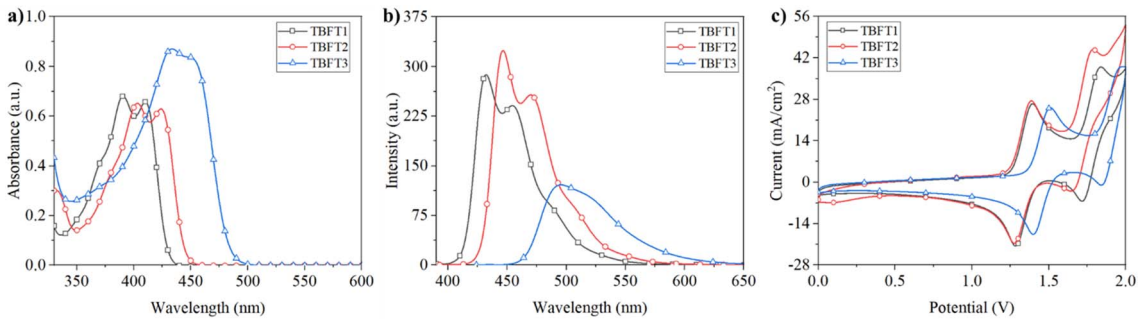

Fig. 2 (a) Absorption and (b) emission spectra of TBFT1–3 in DCM (path length of the cuvette, $l = 1$ cm, 1×10^{-5} M). The excitation wavelength (λ_{ex}) = 390 nm for TBFT1, $\lambda_{ex} = 403$ nm for TBFT2, and $\lambda_{ex} = 433$ nm for TBFT3. (c) Cyclic voltammograms of TBFT1–3 (1×10^{-3} M) in DCM using 0.1 M $TBAPF_6$ as the supporting electrolyte, a glassy carbon electrode as the working electrode, Pt wire as the counter electrode and a calomel electrode as the reference electrode.

Table 1 Optical, photophysical, and electrochemical data of TBFT1–3

Compounds	λ_{abs} [nm]	λ_{em} [nm]	E_g[a] [eV]	E_{ox} [eV]	HOMO[b] [eV]	LUMO[c] [eV]	Φ_f[d]	τ [ns]	k_r[e] [s^{-1}]	K_{nr}[f] [s^{-1}]	K_r/k_{nr}
TBFT1	390	432	2.93	1.26	−5.27	−2.34	0.86	1.54	5.58×10^8	9.13×10^7	6.11
TBFT2	403	446	2.83	1.25	−5.26	−2.43	0.83	1.53	5.42×10^8	1.12×10^8	4.84
TBFT3	433	497	2.60	1.36	−5.37	−2.77	0.42	1.49	2.82×10^8	3.96×10^8	0.72

[a] Optical band gap was calculated from the absorption onset. [b] The HOMO energy levels are calculated from the tangential onset of oxidation (E_{ox}^{onset}) by cyclic voltammetry using the equation: $E_{HOMO} = [-(E_{ox}^{onset} - E_{1/2}^{ferrocene} + 4.8)]$ eV. [c] LUMO levels are estimated from the optical bandgap and HOMO values.[20] [d] Fluorescence quantum yields are determined using quinine sulfate as the standard ($\Phi_f = 0.546$ in 0.1 N H_2SO_4). [e] Radiative decay constant, $k_r = \Phi_f/\tau$. [f] Non-radiative decay constant, k_{nr} calculated by using the equation, $\tau = 1/(k_r + k_{nr})$.[19]

The HOMO values of the regioisomers TBFT1 and TBFT2 are similar, −5.27 eV and −5.26 eV, respectively. However, their LUMO levels differ, −2.34 eV for TBFT1 and −2.43 eV for TBFT2. This difference in energy levels is reflected in their band gap values (E_g). Compared to TBFT1, TBFT2 has a lower E_g value (2.83 eV), shifting the absorption maxima of the latter to a higher wavelength region (403 nm) with a pale-yellow color in the neutral form. Consequently, TBFT1 with a higher E_g value absorbs in the lower wavelength region (390 nm) and appears transparent or colorless. Accordingly, the difference in the energy levels of the regioisomers is reflected in their neutral state color. The presence of an electron-withdrawing group in TBFT3 further reduces the E_g value to 2.60 eV and shifts the absorption maxima even higher to 433 nm. The compound appears as a bright yellow color in the neutral state. Functionalizing the core with different moieties produces molecules with different E_g values due to the electronic effects of the substituents, and as a result, the molecules will have a distinct visual appearance.

The EC properties of the molecules were examined *in situ* by recording the optical transitions in the UV-visible and near-infrared (NIR) regions upon varying the potential from 0 to 2 V. The spectroelectrograms of the electrochromes are depicted in Fig. 3, and the inset shows the photograph of TBFT1–3 in the neutral and colored states. As seen in Fig. 3a–c, the neutral species (at 0 V) absorbs in both UV and visible regions corresponding to σ–σ* and to π–π* transitions, respectively. Upon oxidation, the absorbance of electronic transitions of TBFT1–3 in the UV-visible region began depleting, whereas a new broad absorption band started ascending at around 625 nm, 653 nm, and 635 nm, respectively, as seen in Fig. 3a–c. These new absorption bands indicate the formation of EC radical cations.

An interesting and unexpected aspect of the newly formed species is they have two distinct energy transitions in the visible range since the neutral species absorption does not subside completely upon oxidation. The visual appearance of these charged species varies based on the absorption range of these two-band absorptions. For example, in TBFT1, the neutral state λ_{max} is at 390 nm, which confirms the molecule's colorless nature and the radical cations' λ_{max} is around 625 nm. So, there will not be any color mixing happening in the oxidized species, and this ultimately results in a blue-colored charged state. On the other hand, TBFT2 and TBFT3 are colored in the neutral state, and the applied potential impacts the formation of colored species with different absorption wavelengths, eventually leading to a prominent color mixing.[21]

In the oxidized state, TBFT2 absorbs around 400 nm and 653 nm and finally gives away a bluish-green color due to the combination of pale yellow and blue. TBFT3 visually appears to be a bright green due to the combination of bright yellow and blue. This two-band absorption is rare because it involves controlling two energy transitions in the visible region; one should be short, and the other has to be long-wave absorption. More significantly, the deep valley between these two energy transitions at around 500 nm further benefits the fine-tuning of the green color.[22]

Therefore, it is evident from the spectroelectrochemical studies that by fine-tuning the conjugation by creating a dihedral angle strain (TBFT1) we can devise an EC system that can switch its color from a transparent or colorless state to a vibrant blue color. These sorts of materials are incredibly essential for the fabrication of smart windows. On the other hand, TBFT3, the ADA system made by anchoring the molecular backbone with two electron-withdrawing acetyl groups, resulted in a bright yellow-colored neutral species capable of undergoing two-band energy absorption and delivering a vibrant green-colored state. The materials that trade their optical states from one color to another are potential contenders for simulating sunglasses. Therefore, it is noteworthy that the structural design approach helps to concoct two different types of systems by coupling with simple heterocycles and their derivatives.

The above-mentioned visual appearance of each color was further analyzed by using the absorption spectra of electrodes to obtain the CIE color space values ($L^*a^*b^*$) calculated using a colorimeter. For TBFT1, the a^* and b^* components obtained are −1 and 4 for the neutral species (CIE: 0.32 and 0.34) and −7 and −45 for the charged state (CIE: 0.18 and 0.20). These numerical values affirm the colorless neutral state and blue color of the oxidized form. TBFT2 in the oxidized state delivers negative values for both a^* and b^* and proves its bluish-green appearance (CIE: 0.19 and 0.28), and in the ADA system (TBFT3), the a^* value recedes from −14 to −43 upon oxidation and ascertains the yellow (CIE: 0.42 and 0.50) to green color (CIE: 0.31 and 0.58) change. The $L^*a^*b^*$ values and CIE coordinates of the electrochromes in neutral and colored states are summarized in Table S1,† and for a better understanding of the color tuning, the CIE chart of the compounds is also provided in Fig. S44.†

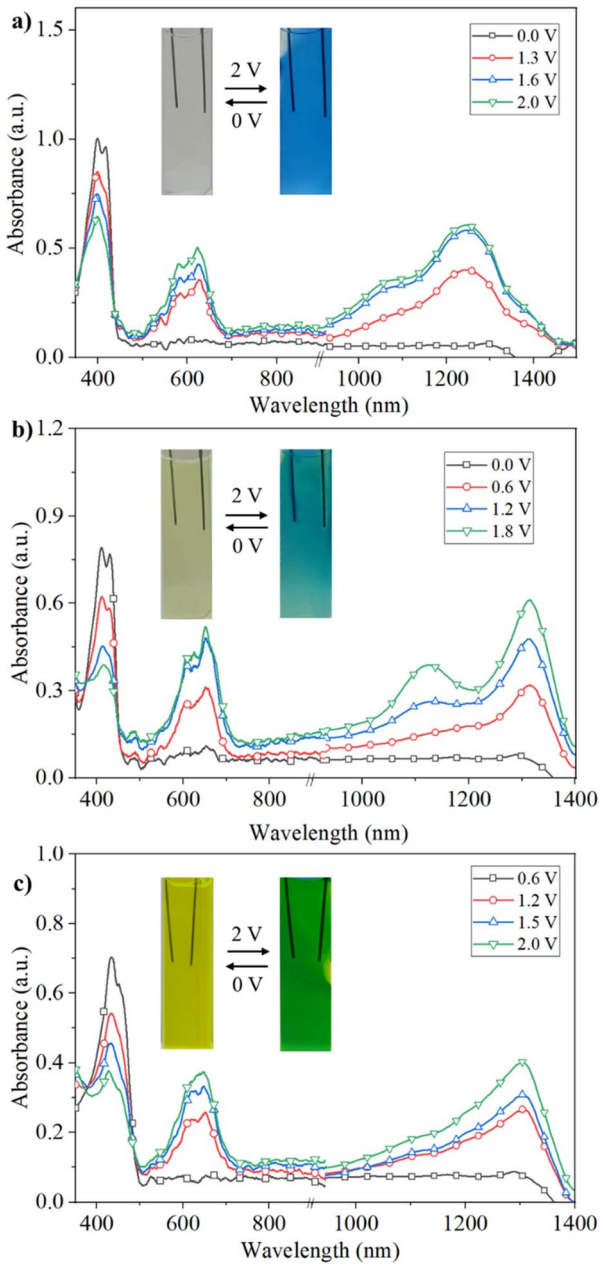

Fig. 3 Spectroelectrochemistry of (a) TBFT1, (b) TBFT2, and (c) TBFT3 in 0.1 M $TBAPF_6$ in DCM at applied potentials carried out with a Pt mesh working electrode, Pt wire counter electrode, and Ag/Ag^+ quasi reference electrode.

The optical properties of the electrochromes have also been examined in the NIR region,[23,24] and the absorption spectra are presented in Fig. 3a–c. From the NIR spectra, it is evident that oxidation of TBFT1–3 resulted in the formation of a broad energy transition centered around λ_{max} of 1230 nm, 1270 nm, and 1240 nm, respectively, which indicates the formation of a low energy charged species, called bications. Thus, the spectroelectrochemistry experiments confirm the EC behavior; moreover, all three electrochromes can absorb light in the UV-visible and NIR regions. These features are essential for smart windows because they can reduce heating inside the buildings by absorbing the NIR region and also provide a protective shield from harmful UV light.

The reaction mechanism of the color change is given below,

$$\text{TBF-Ar} \underset{+e^+}{\overset{-e^-}{\rightleftharpoons}} \text{TBF-Ar}^{+\bullet} \underset{+e^+}{\overset{-e^-}{\rightleftharpoons}} \text{TBF-Ar}^{++}$$

Here, TBF-Ar can be TBFT1/T2/T3; in the neutral state, the molecule does not have any charge and possesses colorless (TBFT1) or yellow colored (TBFT2 and TBFT3) due to its absorption in the UV and UV-visible region respectively. On oxidation, the molecule loses electrons and forms corresponding radical cations, $TBF\text{-}Ar^{+\bullet}$, with a different color due to the absorption of the newly formed species in the visible region. Further oxidation of the radical cationic species produces a bicationic species, TBF^{++}.

2.5 Electrochromic contrast

To demonstrate the optical contrast of the electrochromes, the percentage transmittance changes ($\Delta T\%$) and optical densities (ΔOD) of all the molecules were calculated in the neutral and colored states. By using the following equations, the optical modulation can be determined in terms of transmittance modulation or absorbance modulation: $\Delta T = T_{neutral} - T_{color}$ (where $T_{neutral}$ and T_{color} are the transmittances at the neutral and oxidized states) and $\Delta A = A_{color} - A_{neutral}$ (where A_{color} and $A_{neutral}$ are the absorbances at the fully oxidized and neutral states).[25] $\Delta T\%$ values were plotted over the wavelength range of 350–750 nm, and the transmittance change is shown in Fig. 4a. The less conjugated molecule, TBFT1, gives a more significant shift in the transmittance value of 53% at 624 nm compared to its positional isomer (TBFT2: 48% at 653 nm) and the ADA system (TBFT3: 44% at 635 nm). ΔOD of the compounds is calculated using the equation $\Delta OD = \ln(T_{neutral}/T_{colored})$. The ΔOD of TBFT1 at 625 nm is 1.06, TBFT2 is 0.98 at 653 nm, and TBFT3 is 0.73 at 645 nm. All three electrochromes give a high ΔA value (>0.3), and TBFT1 offers a higher value of 0.42 compared to TBFT2 and TBFT3 (Fig. S39†).

2.6 Response time and coloration efficiencies

A vital quality of EC molecules that one should consider while developing smart devices for real-time applications is their

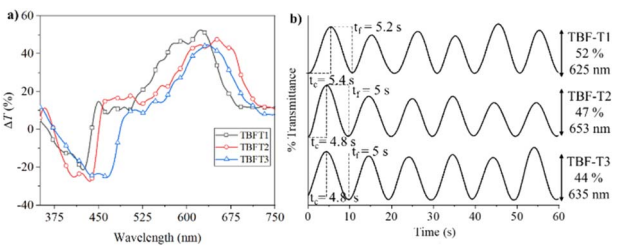

Fig. 4 (a) Percentage transmittance changes ($\Delta T\%$) of the molecules at various wavelengths and (b) EC switching (potential switched between 0–2 V) of TBFT1–3 at radical cation's wavelengths in 0.1 M $TBAPF_6$ in DCM measured using a Pt mesh as the working electrode, Pt wire is taken as the counter electrode and Ag/Ag^+ as the quasi reference electrode with a switching time of 5 s. The coloration time (t_c) and fading time (t_f) of the electrochromes are marked in the figure.

coloration efficiency (CE (η)) and the switching time. CE of an electrochrome can be defined as the ratio of change in optical absorbance (ΔA) for a definite amount of charge injected per unit area (Q), *i.e.*, coloration efficiency (η) = $\Delta A/Q$ cm^2 C^{-1} and the switching time or response time refers to the time required by an electrochrome to completely change from a colored to a neutral state or *vice versa*.[26] The CE of TBFT1–3 is determined by conducting tandem chronoabsorptometry/chronocoulometry experiments (Fig. S41†) in an EC cuvette using a Pt mesh as the working electrode, Ag/Ag$^+$ as the quasi-reference electrode, and Pt wire as the counter electrode in DCM using 0.1 M TBAPF$_6$ as the supporting electrolyte.

The electrode potential is swapped between 0 and 2 V with 5- and 10 seconds intervals and the resultant optical changes are monitored as a function of time at the radical cation wavelength of TBFT1–3 and are depicted in Fig. 4b and S43,† respectively. The color change of the solution-based devices is videographed and provided in the ESI.† TBFT1–3 switches efficiently between the neutral and the colored state with a transmittance change (ΔT%) of 52%, 47%, and 44%, respectively. The coloration efficiency of TBFT1–3 is calculated from the optical density difference and charge involved in the particular electrochemical reaction, and the CE of all three ECs is in a similar range and estimated to be 106, 103, and 100 cm^2 C^{-1} for TBFT1–3, respectively.

2.7 Device fabrication

The materiality of electrochromes in next-generation smart materials exclusively relies upon the nature of the electrolyte medium, the electrodes, and, most importantly, the material's capability to function in all forms. Thus, to explore the potential of the synthesized smart molecules, we tested the functioning of the electrochromes in three states: solution, gel, and solid state. A simple two-electrode configuration was adopted for device fabrication.[27,28]

As shown in the first column of Fig. 5, the solution state ECDs are fabricated by assembling the two FTO-coated glass plates (2.5 cm × 2.5 cm, resistivity = 10 Ω sq^{-1}) and a spacer (250 μm). The components are sealed using UV-curable resin, and the FTO plates function as electrodes. The effective dimension of the device is 1.5 cm × 2.3 cm × 0.25 mm. A solution of the active component, *i.e.*, the electrochromes solution (1×10^{-3} M) and supporting electrolyte (0.1 M TBAPF$_6$), is injected into the space using a syringe, followed by applying the potential and the photographs of the device before and after applying potential are shown in Fig. 5d, g and j. The second column of Fig. 5 illustrates the device working in a gel state. EC gel was prepared by dissolving the respective active material (TBFT1–3), polymethylmethacrylate (PMMA), and TBAPF$_6$ in a solvent mixture containing acetonitrile (ACN) and propylene carbonate (PC) in a ratio of 0.02 : 6.98 : 3:70 : 20 by weight through continuous stirring and mild heating. A frame of double-sided adhesive tape was placed on the conductive side of a pristine 2 cm × 2 cm FTO-coated glass slide. The EC gel was spread inside the frame, and the second FTO glass face-down was placed on the gel-coated slide. The two electrodes were then compelled together. Aluminum foils were used on both sides of the device as electrical contacts to connect to the external power supply.

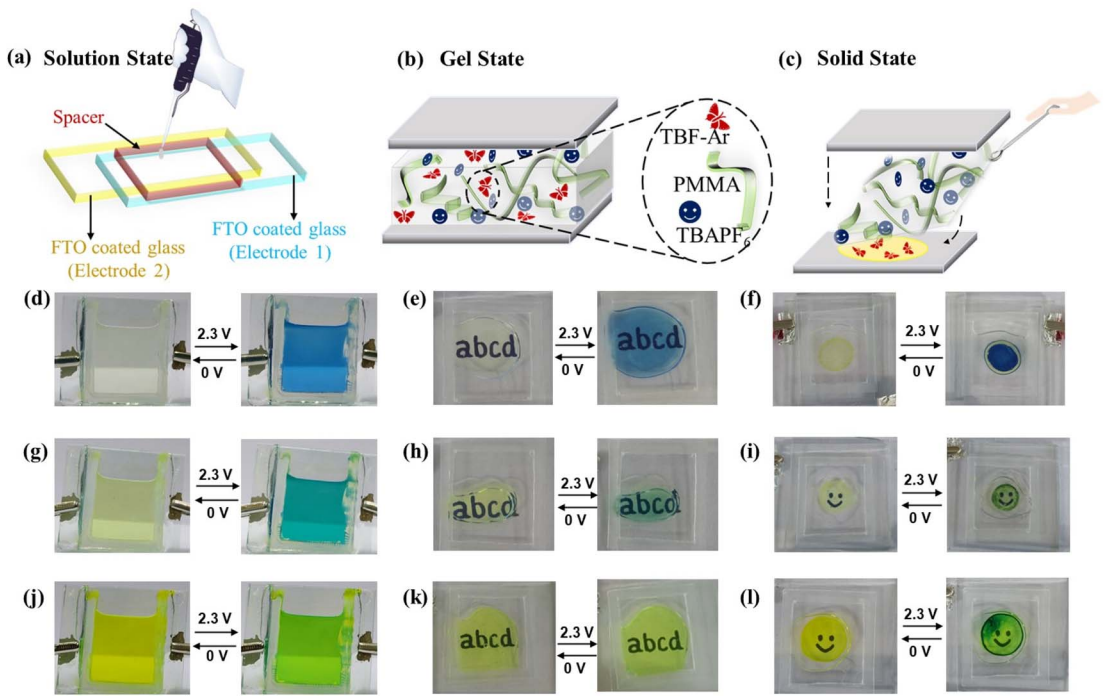

Fig. 5 Schematics of typical EC devices (a) solution state, (b) gel state, and (c) solid state, where FTO substrates are used as the electrode material, the TBFT1–3 as the anodically coloring active material, and TBAPF$_6$ as the supporting electrolyte. Solution-based devices: (d) TBFT1, (g) TBFT2, and (j) TBFT3; gel state: (e) TBFT1, (h) TBFT2, and (k) TBFT3; solid state: (f) TBFT1, (i) TBFT2, and (l) TBFT3.

Similarly, we fabricated the solid-state device by spin-coating the active material on the conducting FTO surface (third column of Fig. 5). A solution of the electrochrome in DCM solvent (1 mg in 0.5 mL DCM) was prepared. The spinning time was set to 50 seconds, and the rotation per minute (RPM) was set to 110–150 and increased to 1000 rpm for 30 seconds. The FTO substrate was then placed on the spinning disc and switched on the vacuum pump. The rotor was switched on, the compound solution was dispensed on the center of the substrate using a dropper, and the resultant EC layer was dried under vacuum at 25 °C for 4 hours. The gel electrolyte was prepared by mixing $TBAPF_6$: PMMA : ACN : PC in a ratio of 3 : 7 : 70 : 20 by weight. The spacer was then placed on top of the spin-coated FTO, followed by applying the electrolyte gel and sandwiching the second FTO. Aluminum foils were used on both sides of the device for electrical contacts.[29] The color change is similar to that observed using a 3-electrode system. In solid-state devices, the active material can be coated on the substrate through different techniques, such as spin coating, drop-casting, or dip-coating. We followed the spin coating technique in the device fabrication and drop casting method in energy storage studies to validate these diverse device fabrication techniques. The device fabrication and studies indicate that these molecules can be effectively used as electrochromes in smart windows and other display applications.

2.8 Energy storage studies

The energy storage properties of the ECDs originate from their ability to store charge from the input current.[30] To evaluate the energy storage characteristics, cyclic voltammetry, open circuit potential (OCP), and galvanostatic charge–discharge (GCD) experiments were carried out using a two-electrode configuration. In this direction, three types of devices were fabricated: (1) the active material was dropcast on the FTO, (2) Nafion was coated on the top of the drop cast layer, and (c) the active material was embedded within a matrix containing PMMA and $TBAPF_6$ (gel state). We fabricated two types of solid-state devices: one with a Nafion coating to prevent the delamination of the active material and the other without any additional coating to test the stability and activity of the electrochromes. In the first two cases, an electrolyte gel consisting of PMMA and $TBAPF_6$ in ACN and PC with a ratio of 3 : 7 : 70 : 20 by weight was applied on the top of the dropcast EC layer (or EC layer coated with Nafion), and then the conducting side of the second FTO was placed. The gel state device was also constructed following the fabrication methods described in Section 2.7. The CVs of the devices at different scan rates are measured and illustrated in Fig. S45–47;† as the scan rate increases (5–500 mV s^{-1}), the current and the area under the curve increase, and in addition to this, the rectangular shape of the CV loop (Fig. 6a) and the triangular shaped GCD curves (Fig. 7a–c) suggest electric double layer capacitor (EDLC) behavior of the devices.[31] A small IR_{drop} was found in all GCD curves, originating from the equivalent series resistance, which includes the interface resistance between the electrolyte and electrode and external contact points.[32] The specific capacitance C_{sp} was calculated (Table S2†) from the GCD curve using the equation, $C_{sp} = I\Delta t/m\Delta V$, where I, Δt, m, and ΔV represent discharging current, discharging time, the mass of the active material, and potential window, respectively.[33] We obtained the highest C_{sp} value, 34.72 mA h g^{-1}, from the TBFT1 dropcast layer device with a Nafion coating and 33.07 mA h g^{-1} from the TBFT2 device in the dropcast form. However, not much research has been reported on organic small molecules as multifunctional EC systems with energy storage ability to compare our

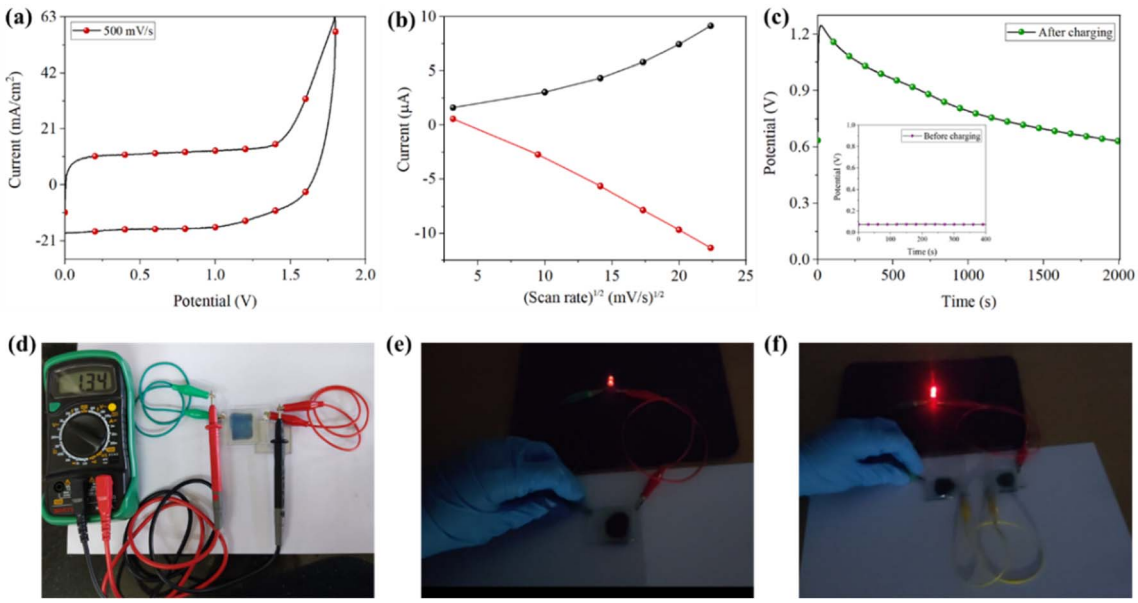

Fig. 6 (a) CV loops obtained from the supercapacitor, (b) current *vs.* square root of scan rate, and (c) OCP of devices fabricated using TBFT1 in the dropcast form. Photographs of the ECD (d) connected to a multimeter after withdrawing the externally applied current, (e and f) during discharging (LED light on) test; the two ECDs in the gel state were connected in series.

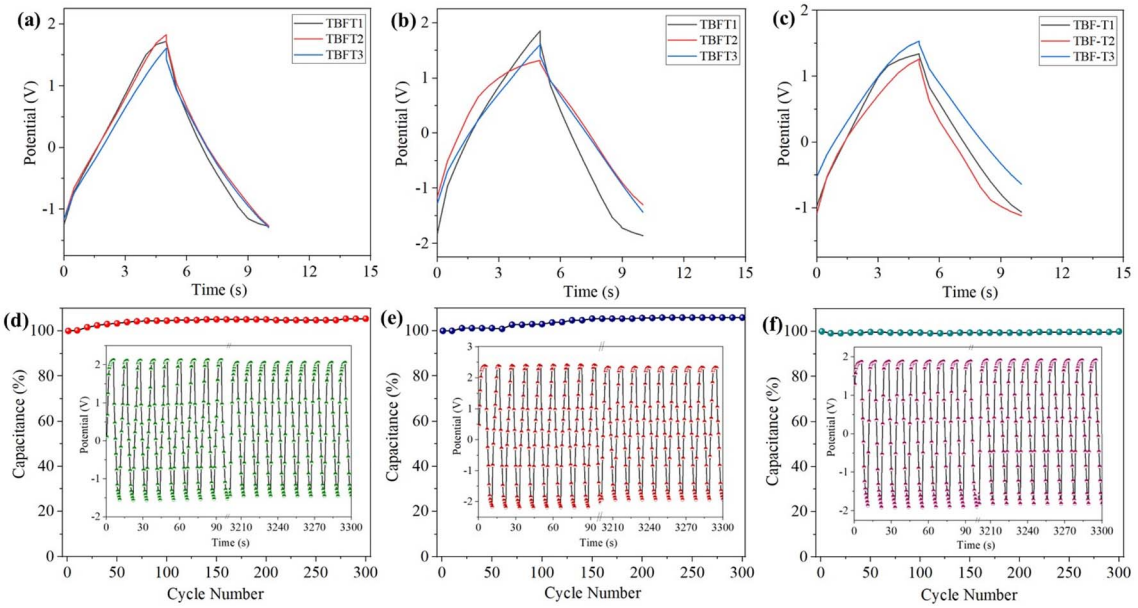

Fig. 7 Galvanostatic charge–discharge curves of the supercapacitors TBFT1–3 (at a current density of 10 A g^{-1}) in the (a) gel state, (b) dropcast form, and (c) dropcast form with a Nafion coating. Cycling stability (300 cycles of continuous charging and discharging) of the supercapacitors derived from TBFT1 in the (d) gel state (c.d. 20 A g^{-1}), (e) dropcast form (c.d. 10 A g^{-1}), and (f) dropcast form with a Nafion coating (50 A g^{-1}).

findings and define our molecules' efficiency and materiality. Liu *et al.* synthesized alkynyl-containing viologen derivatives as the EC unit, and it could serve as the energy storage property with a discharge capacity of 63.6 mA h g^{-1}.[34] Similarly, Sun *et al.* and Zhao *et al.* also studied the charge storage properties of EC viologen and obtained a discharge capacity of 72.2 mA h g^{-1} and areal capacitances of 1.25 mF cm^{-2}.[30,35] However, polymeric or hybrid electrochromic systems have seemed to deliver better energy storage properties.[36–43] In this direction, our research group is currently focusing on developing EC hybrid materials to improve energy storage.

The charge storage performance and operational stability of the ECDs were estimated by executing GCD experiments for 300 cycles, and the devices in all forms displayed excellent performance in terms of rapid charging and discharging, capacitance retention (95–100%), and reversibility, as shown in Fig. 7d–f, S51 and S52.† Moreover, the energy stored in the device can be reutilized to power other electronics; ECD was coupled to a multimeter to prove this. On withdrawing the power supply, the device could hold a potential of 1.34 V, as seen in the multimeter reading (Fig. 6d). When a red light-emitting diode (LED) is connected to a charged device, it emits red light (Fig. 6e and f), and the intensity of the light diminishes as the ECD returns to its original state when the stored energy is completely spent. These observations are affirmed by measuring the devices' open circuit potential (OCP) after charging (Fig. S48–S50†). ECD composed of TBFT1 in all forms provided appealing OCP; the gel state device took 2000 seconds to self-discharge from 1.15 V to 0.83 V. Similarly, the dropcast device potential dropped from 1.24 V to 0.63 V (Fig. 6b), and the dropcast layer with the Nafion coating device produced an OCP of 1.28 V and dropped to 0.48 V in the same period. However, in the gel state, TBFT2 and TBFT3 had OCPs of 0.61 V and 0.49 V, which were reduced to 0.44 V and 0.38 in 2000 seconds. This slow discharging of the devices in the gel state is due to the charged species, presumably tangled within the gel matrix. The results of the GCD and electrochemical experiments infer that the solid-state device with and without the Nafion coating delivers comparable results; thus, the active material does not require any supporting layers to achieve extra stability to the device. The OCPs of the other ECDs are tabulated in Table S2.†

3. Conclusions

We have presented a structural design strategy for developing a unique class of UV to NIR absorbing, anodically coloring, and soluble EC molecules with energy storage properties by anchoring highly conjugated TBF with two regioisomers of thiophenes (TBFT1 and TBFT2) and an electron acceptor 5-acetyl-2-thienyl moiety (TBFT3). The regioisomers displayed distinct EC properties in terms of color; *i.e.*, the 3-thienyl group shifted the absorption towards the UV region and delivered an electrochrome, which is colorless in the neutral state and blue-colored in the oxidized form. In contrast, the 2-thienyl substituted derivative (TBFT2) enhanced the conjugation and thus became pale yellow-colored in the neutral state and blue-green upon oxidation. The ADA system, the TBFT3, showed prominent two-band absorption in the visible region and furnished a vibrant green color on oxidation. Thus, these electrochromes form a potential contender for constructing UV-visible and NIR-absorbing protective smart windows and screens for regulating solar heat gains or cooling down buildings. The EC contrast of all the molecules is more than 40%, with quick reversibility, and the CE is above 100 cm^2 C^{-1}. The molecules

deliver electrochromism in solid, solution, and gel states, thereby enhancing their pertinence. The devices in solid and gel forms can efficiently store imported energy and deliver the stored energy efficiently to power other electronic gadgets, as demonstrated by the LED lighting experiments. The devices discharge very slowly, from 1.2 V to 0.6 V in 2000 s, and show outstanding cycling stability and capacitive retention (95–100%). The new invention reported here, consisting of fused polyaromatic molecules, may revitalize the field of concocting multifunctional ECDs for electrochemical energy storage applications. Our research is currently focused on creating efficient EC molecules with all essential qualities of the EC system with energy storage traits by producing TBF-based small organic molecules and organic–inorganic hybrid systems.

Author contributions

Panichiyil V. Navya: conceptualization, formal analysis, investigation, methodology, project administration, and writing the original draft. Srinivasan Sampath: project administration, resources, supervision, validation, visualization, and writing – review & editing.

Conflicts of interest

There are no conflicts to declare.

Acknowledgements

We thank Dr S. Gokulnath and Dr A. Muthukrishnan, IISER Trivandrum, for extending support to carry out spectroelectrochemistry and GCD experiments. We thank Krithika Ganesan, University of Antwerp, Department of Chemistry, MOSAIC Research group, Belgium, for the computational studies. We also thank Dr A. A. Boopathi, University of Fribourg, for the technical discussions. We also acknowledge the technical support received from the Chemistry and Physics Departments of CUTN. We acknowledge support from IITB for Mass spectrometry and Dr Sundaravel, Bharathiyar University, for TGA studies.

References

1 P. S. Badwal Sukhvinder, S. S. Giddey, C. Munnings, A. I. Bhatt and A. F. Hollenkamp, Emerging electrochemical energy conversion and storage technologies, *Front. Chem.*, 2014, **2**, 2296–2646.
2 V. Augustyn, P. Simon and B. Dunn, Pseudocapacitive Oxide Materials for High-Rate Electrochemical Energy Storage, *Energy Environ. Sci.*, 2014, **7**, 1597–1614.
3 G. A. Corrente, E. Fabiano, F. Manni, G. Chidichimo, G. Gigli, A. Beneduci and A.-L. Capodilupo, Colorless to All-Black Full-NIR High-Contrast Switching in Solid Electrochromic Films Prepared with Organic Mixed Valence Systems Based on Dibenzofulvene Derivatives, *Chem. Mater.*, 2018, **30**, 5610–5620.
4 P. Yang, P. Sun and W. Mai, Electrochromic Energy Storage Devices, *Mater. Today*, 2015, **19**, 394–402.
5 G. Yang, Y.-M. Zhang, Y. Cai, B. Yang, C. Guab and S. X.-A. Zhang, Advances in Nanomaterials for Electrochromic Devices, *Chem. Soc. Rev.*, 2020, **49**, 8687–8720.
6 C. Gu, A.-B. Jia, Y.-M. Zhang and S. X.-A. Zhang, Emerging Electrochromic Materials and Devices for Future Displays, *Chem. Rev.*, 2022, **122**, 14679–14721.
7 G. Sonmez, H. Meng, Q. Zang and F. A. Wudl, Highly Stable, A New Electrochromic Polymer: poly (1,4-bis(2-(3′4′-ethylenedioxy)thienyl)-2-methoxy-5-2″ ethylhexyloxybenzene), *Adv. Funct. Mater.*, 2003, **13**, 726–731.
8 M. Sassi, M. M. Salamone, R. Ruffo, C. M. Mari, G. A. Pagani and L. Beverina, Gray to Colorless Switching, Crosslinked Electrochromic Polymers with Outstanding Stability and Transmissivity From Naphthalenediimmide-Functionalized EDOT, *Adv. Mater.*, 2012, **24**, 2004–2008.
9 P. M. Beaujuge, S. Ellinger and J. R. Reynolds, The Donor–Acceptor Approach Allows a Black-to-Transmissive Switching Polymeric Electrochrome, *Nat. Mater.*, 2008, **7**, 795–799.
10 C. M. Amb, P. M. Beaujuge and J. R. Reynolds, Spray-Processable Blue-to-Highly Transmissive Switching Polymer Electrochromes *via* the Donor–Acceptor Approach, *Adv. Mater.*, 2010, **22**, 724–728.
11 J. Gao, D.-G. Liu, J.-M. Sansinena and H.-L. Wang, Synthesis and Characterization of Electrochromic Polyamide with Well-Defined Molecular Structures and Redox Properties, *Adv. Funct. Mater.*, 2004, **14**, 537–543.
12 M. Li, A. Patra, Y. Sheynin and M. Bendikov, Hexyl-Derivatized Poly(3,4-ethylenedioxyselenophene): Novel Highly Stable Organic Electrochromic Material with High Contrast Ratio, High Coloration Efficiency, and Low-Switching Voltage, *Adv. Mater.*, 2009, **21**, 1707–1711.
13 P. M. Beaujuge, S. Ellinger and J. R. Reynolds, Spray Processable Green to Highly Transmissive Electrochromics *via* Chemically Polymerizable Donor–Acceptor Heterocyclic Pentamers, *Adv. Mater.*, 2008, **20**, 2772–2776.
14 A. M. Osterholm, L. Nhon, D. E. Shen, A. M. Dejneka, A. L. Tomlinson and J. R. Reynolds, Conquering Residual Light Absorption in the Transmissive States of Organic Electrochromic Materials, *Mater. Horiz.*, 2022, **9**, 252–260.
15 H.-J. Yen, C.-J. Chen and G.-S. Liou, Flexible Multi-Colored Electrochromic and Volatile Polymer Memory Devices Derived from Starburst Triarylamine-Based Electroactive Polyimide, *Adv. Funct. Mater.*, 2013, **23**, 5307–5316.
16 M. Sassi, M. M. Salamone, R. Ruffo, G. E. Patriarca, C. M. Mari, G. A. Pagani, U. Posset and L. Beverina, State-of-the-Art Neutral Tint Multichromophoric Polymers for High-Contrast See-Through Electrochromic Devices, *Adv. Funct. Mater.*, 2016, **26**, 5240–5246.
17 A. A. Boopathi, S. Sampath and T. Narasimhaswamy, Isothermal and Non-Isothermal Cold Crystallization of Tetrabenzofluorene (TBF) Molecules, *New J. Chem.*, 2019, **43**, 9500–9506.

18 S. Sampath, A. A. Boopathi and A. B. Mandal, "Bottom-up" Self-Assembly and "Cold Crystallization" of Butterfly Shaped Tetrabenzofluorene Molecules, *Phys. Chem. Chem. Phys.*, 2016, **18**, 21251–21258.

19 A. Ajayaghosh, V. K. Praveen, S. Srinivasan and R. Varghese, Quadrupolar p-Gels: Sol–Gel Tunable Red–Green–Blue Emission in Donor–Acceptor-Type Oligo(p-phenylenevinylene)s, *Adv. Mater.*, 2007, **19**, 411–415.

20 Y. Li, D. H. Lee, J. Lee, T. L. Nguyen, S. Hwang, M. J. Park, D. H. Choi and H. Y. Woo, Two Regioisomeric π-Conjugated Small Molecules: Synthesis, Photophysical, Packing, and Optoelectronic Properties, *Adv. Funct. Mater.*, 2017, **27**, 1701942.

21 C. M. Amb, A. L. Dyer and J. R. Reynolds, Navigating the Color Palette of Solution-Processable Electrochromic Polymers, *Chem. Mater.*, 2011, **23**, 397–415.

22 G. Sonmez, C. K. F. Shen, Y. Rubin and F. Wudl, A Red, Green, and Blue (RGB) Polymeric Electrochromic Device (PECD): The Dawning of the PECD Era, *Angew. Chem., Int. Ed.*, 2004, **43**, 1497–1502.

23 N. C. Davy, M. Sezen-Edmonds, J. Gao, X. Lin, A. Liu, N. Yao, A. Kahn and Y. Loo, Pairing of Near-Ultraviolet Solar Cells with Electrochromic Windows for Smart Management of the Solar Spectrum, *Nat. Energy*, 2017, **2**, 17104.

24 G. A. Corrente, D. A. González, E. Aktas, A. L. Capodilupo, G. Mazzone, F. Ruighi, G. Accorsi, D. Imbardelli, C. Rodriguez-Seco, E. Martinez-Ferrero, E. Palomares and A. Beneduci, Vis–NIR Electrochromism and NIR–Green Electroluminochromism in Dual Functional Benzothiadiazole-Arylamine Mixed-Valence Compounds, *Adv. Opt. Mater.*, 2023, **11**, 2201506.

25 C.-G. Wu, M.-I. Lu, S.-J. Chang and C.-S. Wei, A Solution-Processable High-Coloration-Efficiency Low-Switching-Voltage Electrochromic Polymer Based on Polycyclopentadithiophene, *Adv. Funct. Mater.*, 2007, **17**, 1063–1070.

26 P. M. Beaujuge and J. R. Reynolds, Color Control in π-Conjugated Organic Polymers for Use in Electrochromic Devices, *Chem. Rev.*, 2010, **110**, 268–320.

27 M. Stolar, J. Borau-Garcia, M. Toonen and T. Baumgartner, Synthesis and Tunability of Highly Electron-Accepting, N-Benzylated "Phosphaviologens", *J. Am. Chem. Soc.*, 2015, **137**, 3366–3371.

28 C. Reus, M. Stolar, J. Vanderkley, J. Nebauer and T. Baumgartner, A Convenient N-Arylation Route for Electron-Deficient Pyridines: The Case of π-Extended Electrochromic Phosphaviologens, *J. Am. Chem. Soc.*, 2015, **137**, 11710–11717.

29 A. A. Argun, A. Cirpan and J. R. Reynolds, The First Truly All-Polymer Electrochromic Devices, *Adv. Mater.*, 2003, **15**, 1338–1341.

30 J. Wang, L. Zhang, L. Yu, Z. Jiao, H. Xie, X. W. Lou and X. W. Sun, A Bi-Functional Device for Self-Powered Electrochromic Window and Self-Rechargeable Transparent Battery Applications, *Nat. Commun.*, 2014, **5**, 4921.

31 B. Pandit, D. P. Dubal, P. Gómez-Romero, B. B. Kale and B. R. Sankapal, V_2O_5 encapsulated MWCNTs in 2D surface architecture: Complete Solid-State Bendable Highly Stabilized Energy Efficient Supercapacitor Device, *Sci. Rep.*, 2017, **7**, 43430.

32 O. Eisenberg, Y. M. Algavi, H. Weissman, J. Narevicius, B. Rybtchinski, M. Lahav and M. E. van der Boom, Dual Function Metallo–Organic Assemblies for Electrochromic–Hybrid Supercapacitors, *Adv. Mater. Interfaces*, 2020, 2000718.

33 R. Yuksel, S. C. Cevher, A. Cirpan, L. Toppare and H. E. Unalan, All-Organic Electrochromic Supercapacitor Electrodes, *J. Electrochem. Soc.*, 2015, **162**, 2805–2810.

34 H. Ling, J. Wu, F. Su, Y. Tian and Y. J. Liu, Automatic Light-Adjusting Electrochromic Device Powered by Perovskite Solar Cell, *Nat. Commun.*, 2021, **12**, 1010.

35 Y. Zhuang, W. Zhao, L. Wang, F. Li, W. Wang, S. Liu, W. Huang and Q. Zhao, Soluble Triarylamine Functionalized Symmetric Viologen for All-Solid-State Electrochromic Supercapacitors, *Sci. China: Chem.*, 2020, **63**, 1632–1644.

36 K. Wang, H. Wu, Y. Meng, Y. Zhanga and Z. Wei, Integrated Energy Storage and Electrochromic Function in One Flexible Device: An Energy Storage Smart Window, *Energy Environ. Sci.*, 2012, **5**, 8384–8389.

37 G. Cai, J. Chen, J. Xiong, A. Lee-Sie Eh, J. Wang, M. Higuchi and P. S. Lee, Molecular Level Assembly for High-Performance Flexible Electrochromic Energy-Storage Devices, *ACS Energy Lett.*, 2020, **5**, 1159–1166.

38 H. Li, L. McRae, C. J. Firby and A. Y. Elezzabi, Rechargeable Aqueous Electrochromic Batteries Utilizing Ti-Substituted Tungsten Molybdenum Oxide Based Zn^{2+} Ion Intercalation Cathodes, *Adv. Mater.*, 2019, **31**, 1807065.

39 T. Y. Yun, X. Li, S. H. Kim and H. C. Moon, Dual-Function Electrochromic Supercapacitors Displaying Real-Time Capacity in Color, *ACS Appl. Mater. Interfaces*, 2018, **50**, 43993–43999.

40 M. Indulekha, P. M. Anjana, N. Anjali, P. Dipak, A. S. Priyanka, S. P. Renjith, R. B. Rakhi, S. Sreejith and A. Ajayaghosh, Tunable Capacitive Behavior in Metallopolymer-based Electrochromic Thin Film Supercapacitors, *ACS Appl. Mater. Interfaces*, 2022, **14**, 31900–31910.

41 S. Ming, K. Lin, H. Zhang, F. Jiang, P. Liu, J. Xu, G. Nie and X. Duan, Electrochromic Polymers with Multiple Redox Couples Applied to Monitor Energy Storage States of Supercapacitors, *Chem. Commun.*, 2020, **56**, 5275–5278.

42 P. Yang, P. Sun, Z. Chai, L. Huang, X. Cai, S. Tan, J. Song and W. Mai, Large-Scale Fabrication of Pseudocapacitive Glass Windows that Combine Electrochromism and Energy Storage, *Angew. Chem., Int. Ed.*, 2014, **53**, 1–6.

43 B. Wang, L. Wang, H. Chen, Y. Jia and Y. Ma, Electropolymerized Triphenylamine Network Films for High-Performance Transparent to Black Electrochromism and Capacitance, *Adv. Opt. Mater.*, 2023, **11**, 2201572.